Earth and Planetary Science Letters 543 (2020) 116345

Contents lists available at ScienceDirect

Earth and Planetary Science Letters

www.elsevier.com/locate/epsl

The seismically fastest chemical heterogeneity in the Earth's deep upper mantle—implications from the single-crystal thermoelastic properties of jadeite

Ming Hao [a,b,*], Jin S. Zhang [a,b,*], Caroline E. Pierotti [a,c], Wen-Yi Zhou [a,b], Dongzhou Zhang [d,e], Przemyslaw Dera [d]

[a] Department of Earth and Planetary Sciences, University of New Mexico, Albuquerque, NM 87131, United States of America
[b] Institute of Meteoritics, University of New Mexico, Albuquerque, NM 87131, United States of America
[c] Albuquerque High School, Albuquerque, NM 87102, United States of America
[d] Hawaii Institute of Geophysics and Planetology, University of Hawaii at Manoa, HI 96822, United States of America
[e] GeoSoilEnviroCARS, University of Chicago, Argonne National Laboratory, Argonne, IL 60439, United States of America

ARTICLE INFO

Article history:
Received 6 October 2019
Received in revised form 27 April 2020
Accepted 13 May 2020
Available online 26 May 2020
Editor: M. Ishii

Keywords:
single-crystal elasticity
seismic velocity
continent-derived sediments/crust
enriched geochemical reservoirs
jadeite

ABSTRACT

Jadeite is a major mineral phase (up to 50 vol%) in the subducted sediments/crust with continental origin, which are one of the major heterogeneities and important enriched geochemical reservoirs (such as EM-1 and EM-2) for incompatible elements in the Earth's interior. Identifying and locating the enriched geochemical heterogeneities requires knowledge of the elastic properties of relevant mineral phases at high pressure-temperature conditions. Unfortunately, the single-crystal elastic properties of jadeite have never been measured at high-pressure conditions, partially due to its low crystal symmetry. In this study, we have experimentally determined the single-crystal elastic moduli of jadeite at high pressures for the first time up to 18 GPa at the ambient temperature condition using Brillouin spectroscopy. Fitting the third-order finite strain equation of state to the velocity-pressure data yields K'_{S0}=3.9(1), G'_0=1.09(4) with ρ_0=3.302(5) g/cm^3, K_{S0}=138(3) GPa, and G_0=84(2) GPa. In addition, we have also conducted synchrotron single-crystal X-ray diffraction experiments up to 25 GPa and 700 K. The fitting of a Holland-Powell type thermal-pressure Birch-Murnaghan equation of state yields K'_{T0}=3.8(2) and α_0=3.4(5) $\times 10^{-5}$ K^{-1}. Based on the obtained thermoelastic parameters of jadeite, the density and seismic velocities of continent-derived sediments/crust are modeled at the depth range from 200 to 500 km. The seismic velocities of the subducted continental sediments/crust become extremely fast at depths greater than ~300 km, up to 11.8% and 14.7% faster than the Vp and Vs of the ambient mantle, and 5.6% and 7.3% faster than the Vp and Vs of the subducted oceanic crust. The existence of even a small amount of the subducted continental sediments/crust can result in strong seismic anomalies in the Earth's interior.

© 2020 Elsevier B.V. All rights reserved.

1. Introduction

Jadeite ($NaAlSi_2O_6$) is a major mineral phase (up to 50 vol%) in the subducted sediments/crust with continental origin and can exist up to 500 km depth in the Earth's interior (Irifune et al., 1994; Wu et al., 2009). The geochemical data, especially isotopic and trace-element geochemistry of oceanic island basalts (OIB), show that the subducted continental sediments/crust are one of the major enriched geochemical heterogeneities in the Earth's mantle (Hofmann, 1997). In particular, the enriched mantle 1 (EM-1) sources are consistent with the recycled ancient continental sediments/crust and the enriched mantle 2 (EM-2) sources are polluted by continent-derived sediments (e.g. Chauvel et al., 1992). Both EM-1 and EM-2 are the main geochemical reservoirs for the incompatible elements (e.g. U, Th, and K) and isotopes (e.g. ^{143}Nd, ^{87}Sr, and ^{40}Ar) in the Earth's interior (e.g. Hofmann, 1997). The enriched geochemical reservoirs have important geophysical implications as well. For example, the enrichment of K plays a significant role in the thermal evolution of the Earth (e.g. Arevalo et al., 2009). Considering the incompatible nature of K, continental crust and the continent-derived sediments on the ocean floor are the primary sources of the K in the Earth's interior, in addition to the possible important primitive K reservoirs formed early in the Earth's history (e.g. Corgne et al., 2007). Therefore, identification of the subducted

* Corresponding authors at: Department of Earth and Planetary Sciences, University of New Mexico, Albuquerque, NM 87131, United States of America.
E-mail addresses: minghao@unm.edu (M. Hao), jinzhang@unm.edu (J.S. Zhang).

https://doi.org/10.1016/j.epsl.2020.116345
0012-821X/© 2020 Elsevier B.V. All rights reserved.

sediments/crust in the mantle is crucial for both the geochemical and geophysical evolution of the Earth (e.g. Kufner et al., 2016).

Seismology provides by far the most precise images of the Earth's interior. Identifying the locality and estimating the size of the subducted continental sediments/crust in the Earth's interior requires the knowledge of the elastic properties of all the relevant mineral phases, especially jadeite, due to its high volume fraction (Irifune et al., 1994; Wu et al., 2009). Previous studies have suggested the possible fast seismic velocities of the subducted continental sediments/crust in the deep upper mantle in presence of stishovite (e.g. Kawai and Tsuchiya, 2015). However, if jadeite is acoustically very slow at high-pressure (P) conditions, due to its abundance (Irifune et al., 1994; Wu et al., 2009), the continental sediments/crust can be seismically slow even with stishovite's presence. In addition, constraining the thermoelastic properties of jadeite is also helpful for modeling the velocity profiles of the subducted oceanic slab crust, considering the fact that the seismic velocities of the slab crust also strongly depend on the molar fraction of the jadeite component in the eclogitic omphacite crystals (Hao et al., 2019a). Thus, in order to model the seismic properties of these geochemical heterogeneities in the Earth's interior, measurements of the single-crystal thermoelastic properties of jadeite under relevant P-temperature (T) conditions are necessary.

Previous equation of state (EOS) studies of jadeite are limited in both P and T (e.g. Zhao et al., 1997; Cameron et al., 1973; Nestola et al., 2006; McCarthy et al., 2008; Tribaudino et al., 2008; Posner et al., 2014; Pandolfo et al., 2015). For example, Posner et al. (2014) performed single-crystal X-ray diffraction (XRD) measurements of jadeite up to 30.4 GPa at 300 K. Pandolfo et al. (2015) measured the thermal expansion coefficients of jadeite up to 1073 K at 1 atm. Zhao et al. (1997) performed the only in situ high P-T EOS study for polycrystalline jadeite up to 8.2 GPa, which is not enough to cover its entire stability range in the Earth's upper mantle. On the other hand, as the acoustically fastest chemical endmember of Clinopyroxene (Cpx), the single-crystal elastic properties of jadeite have been only experimentally determined at ambient condition (Kandelin and Weidner, 1988; Hao et al., 2019a; Norris, 2008) or computed at 0 K and high-P conditions using first-principles calculation (Kawai and Tsuchiya, 2010; Walker, 2012).

Therefore, in this study, we conducted single-crystal Brillouin spectroscopy measurements of natural jadeite crystals up to 18 GPa 300 K at the high-P laser spectroscopy laboratory at University of New Mexico (UNM), and also investigated the thermal EOS of jadeite by performing synchrotron single-crystal XRD experiments on the same crystals up to 25 GPa and 700 K at GeoSoilEnviroCARS (GSECARS), Advanced Photon Source (APS), Argonne National Laboratory (ANL). We then calculated the seismic properties of the subducted oceanic crust and continent-derived sediments/crust using the thermoelastic properties of all relevant phases determined in this and previous studies.

2. Experimental methods

The jadeite crystals (space group $C2/c$) were hand-picked from a natural jadeitite. The chemical composition of the jadeite crystals was determined using a JEOL 8200 Electron Microprobe with 20 nA beam current and 15 kV accelerating voltage at the Institute of Meteoritics, UNM. The composition was determined as $Na_{0.954}Mg_{0.021}Ca_{0.029}Fe_{0.019}Al_{0.966}Si_{2.002}O_6$. Table S1 shows the detailed analysis results. The selected crystals were then double-side polished into platelets with ~15 μm thickness. They were scratch-free under optical examination. The polished samples were then cut into pieces with ~45 μm width for diamond anvil cell (DAC) loading.

Symmetric piston-cylinder DACs and BX90 DACs with standard 60° and 90° opening WC backing seats and 300-350 μm cutlet diamonds were used for Brillouin and XRD experiments. Re gaskets were pre-indented to 45-55 μm thickness. 210-235 μm diameter holes were drilled into the pre-indented gaskets and served as sample chambers. Neon was gas-loaded as the P-transmitting medium at GSECARS, APS, ANL. Gold EOS was used for estimating the experimental Ps for XRD measurements (Fei et al., 2007). For Brillouin measurements, 2 ruby spheres were loaded into each DAC and used as the P standard (Mao et al., 1978). The P differences between the Ps measured from the 2 ruby spheres before and after the completion of the Brillouin scattering measurements at 13 different crystallographic angles of each individual run were smaller than 0.2 GPa.

High-P single-crystal XRD experiments were carried out at GSECARS experimental station 13-BM-C. The X-ray opening angles for symmetric piston-cylinder DACs and BX90 DACs are ±14° and ±24°, respectively. The X-ray beam energy is 28.6 keV and the beam size is ~12 μm × 18 μm. A MAR165 Charge Coupled Device placed on a dedicated rotational arm was used as the detector. NIST standard LaB_6 powder was used to calibrate the detector geometry parameters. 2 different detector positions were used: one was perpendicular to the incident X-ray beam and the other was rotated about the horizontal axis by 20°. We collected both the wide-scan and 1°/step step-scan images with 2 s/° exposure time.

For measurements at ambient condition, the polished platelike crystals were oriented with their plane normals parallel to the incoming X-ray beam. The averaged unit cell parameters from the measured 3 crystals at ambient condition were: a=9.439(5) Å, b=8.583(4) Å, c=5.228(1) Å, and β=107.50(2)°. The calculated ambient density ρ_0 was 3.302(5) g/cm^3. The plane normals of the measured 3 samples were (-0.692, -0.714, 0.106), (0.116, 0.993, -0.021), and (-0.905, 0.302, 0.302). The angular uncertainties were approximately 0.5°. For high P-T single-crystal XRD measurements, we used Pt heaters to heat the sample chamber to 373 K, 500 K, and 700 K at high-P conditions. 2 K-type thermocouples were attached to the diamonds to measure the T. The difference between the 2 T readings was always smaller than 10 K up to the maximum experimental T of 700 K.

Brillouin spectroscopy experiments were performed at the high-P laser spectroscopy laboratory at UNM. The light source was a 300 mW 532 nm single-mode diode-pumped solid-state laser. The measurements were carried out using a 50° symmetric forward scattering geometry. Using a standard silica glass Corning 7980, the scattering angle was calibrated to be 50.42(5)°. The fast and slow directions of the 2 diamond anvils were oriented to match each other. We used the 3 pre-oriented jadeite crystals for the Brillouin measurements at 7 different Ps. To avoid any geometrical errors, compressional (Vp) and shear (Vs) velocities were measured at 13 different Chi angles (0, 30, 60, 90, 120, 150, 180, 195, 225, 255, 285, 315, 345) along the 360° azimuth at each P. All Brillouin spectra show excellent signal-to-noise ratios. Figure S1 shows a typical Brillouin spectrum collected at 18 GPa.

3. Results and discussion

3.1. Thermal EOS of jadeite

Using the ATREX IDL software package (Dera et al., 2013), the single-crystal XRD images were analyzed to obtain the unit cell parameters at each P-T condition (Table S2). Then we performed thermal EOS fit of the obtained unit cell volumes. The conventional isothermal EOS (e.g. Birch-Murnaghan EOS) assumed constant $\partial K_T/\partial T$ and K'_T in the P-T space, which is thermodynamically problematic because $\partial K_T/\partial T = 0$ at T=0 K and K'_T should increase with T (Angel et al., 2018). Thus, the EOS used in this study was modified based on the Birch-Murnaghan EOS with the isochoric thermal-P correction term from Holland and Powell (2011). The

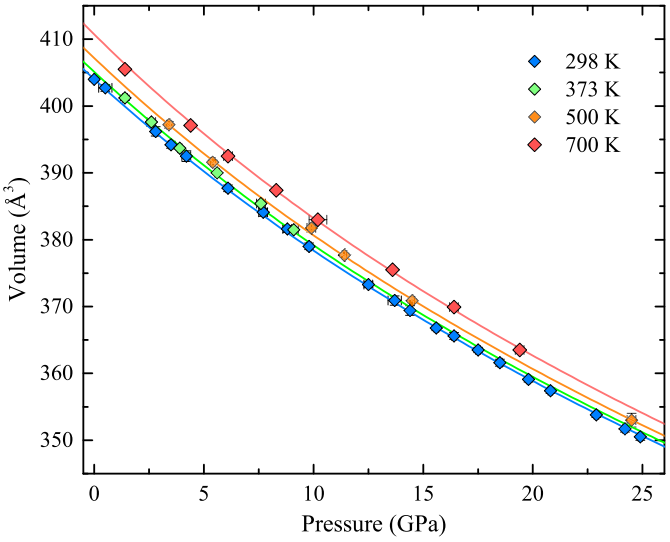

Fig. 1. P-V-T EOS of jadeite with calculated isothermal compression curves.

details of the thermal-P EOS are summarized in the Supporting Information Text S1.1 (Equation S1-S3).

The well-known trade-offs between the ambient isothermal bulk modulus K_{T0} and its P derivative K'_{T0} resulted in the large variations in previous studies, with K_{T0} and K'_{T0} ranging from 125 GPa, 5.0 to 136 GPa, 3.3, respectively (Zhao et al., 1997; Nestola et al., 2006; McCarthy et al., 2008; Posner et al., 2014). Therefore, in this study, we fixed K_{T0} to 134.6 GPa based on the Reuss bound of the adiabatic bulk modulus $K_{S0}{}^R$ determined from high-precision Brillouin spectroscopy experiments (Supporting Information, Text S1.2, Equation S4). With fixed V_0 and K_{T0}, the thermal EOS fitting yielded K'_{T0}=3.8(2) with α_0=3.4(5) $\times 10^{-5}$ K^{-1} (Fig. 1). Compared with previous studies, α_0 is slightly higher whereas K'_{T0} is in the middle of the range determined from previous studies (Nestola et al., 2006; McCarthy et al., 2008; Posner et al., 2014; Zhao et al., 1997; Figure S2).

3.2. High-P single-crystal elastic properties of jadeite

The best-fit values for the 13-independent elastic moduli (C_{ij}) of jadeite at ambient condition were obtained using a least-squares inversion of the Christoffel equation with known ρ_0. The root-mean-square (RMS) residuals between the observed and modeled velocities of the results were less than 50 m/s. The ambient adiabatic bulk (K_{S0}) and shear moduli (G_0) were calculated using the Voigt-Reuss-Hill (VRH) averaging scheme. The high-P densities and elastic properties were iteratively calculated. First, using the least-squares inversion of the Christoffel equation, the C_{ij}s, K_S, G, Vp, and Vs can be calculated at each P with an initial guess of the sample's density. The Vp and Vs are independent of the assumed density values and therefore represent the true high-P aggregate velocities. Fixing ρ_0, K_{S0}, and G_0 to 3.302(5) g/cm^3, 138(3) GPa, and 84(2) GPa, respectively, we can then use the 3rd order finite-strain EOS to fit the P-Vp-Vs data to obtain the P derivatives of K_S and G, as well as the true high-P densities (Davies and Dziewonski, 1975). Finally, we updated the high-P C_{ij}s, K_S, and G with true densities. For low symmetry minerals, such as monoclinic jadeite, it is essential to choose the proper combination of crystallographic orientations in order to reliably invert the full single-crystal C_{ij}s. Therefore, we performed the inversion sensitivity test for the 13 C_{ij}s using the velocities measured along the 39 different crystallographic directions. All the technical details are shown in the Supporting Information Text S1.3, Equation S5. The sensitivity test results are shown in Figure S3. According to Figure S3, the only C_{ij} that can be improved with more measurements along more crystallographic directions is C_{15}, which plays a very minor role in calculating the anisotropic aggregate elastic properties. Figure S4 shows the measured velocities and the calculated velocities from the best-fit C_{ij} model at 18 GPa, and the RMS error is 32 m/s. All the Vp, Vs, C_{ij}s, K_S, G, and density values at each P are listed in Table 1.

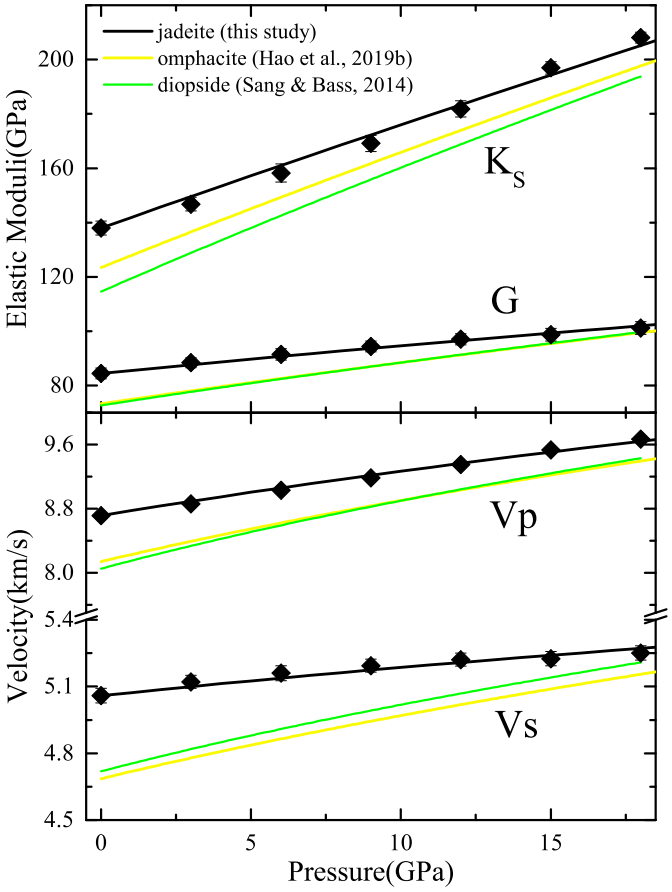

Fig. 2. The high-P K_S, G, Vp, and Vs of jadeite in this study are compared with diopside (Sang and Bass, 2014) and omphacite (Hao et al., 2019b).

The K'_{S0} and G'_0 were determined to be 3.9(1), 1.09(4) with fixed ρ_0=3.302(5) g/cm^3, K_{S0}=138(3) GPa, and G_0=84(2) GPa. The K'_{S0} is consistent with K'_{T0} considering their experimental uncertainties. The K_S, G, Vp, and Vs of jadeite, omphacite, and diopside at different Ps are plotted together in Fig. 2 for comparison (Hao et al., 2019b; Sang and Bass, 2014). We chose to plot the elasticity data measured using Brillouin spectroscopy method only for consistency, although the experimental results obtained using other experimental methods do not deviate far away from the values determined by Brillouin spectroscopy (e.g. sound velocities of diopside determined by Li and Neuville (2010) and Sang and Bass (2014) agree with each other very well). As shown in Fig. 2, jadeite is clearly the fastest Cpx endmember for both Vp and Vs in the entire P range of this study.

Comparing the velocities of all the major upper mantle minerals with jadeite (Figure S5), olivine and pyroxenes are all acoustically slower. It is worth noting that there are some discrepancies between previous EOS and elasticity studies of olivine when the P significantly exceeds its P stability range (Angel et al., 2018). However, within the P range we were modeling in this study, the difference is very small. Stishovite, as expected by its dense structure with 6 coordinated Si, is the fastest mineral phase. The Vp of jadeite is slightly slower than the garnet, whereas its Vs exceeds

Table 1
Single-crystal and aggregate elastic properties of jadeite at different Ps determined in this study.

	1 atm	3.0(1) GPa	6.0(1) GPa	9.0(1) GPa	12.0(1) GPa	15.0(1) GPa	18.0(1) GPa
ρ (g/cm^3)	3.302(5)	3.372	3.437	3.5	3.56	3.617	3.671
C_{11} (GPa)	265.4(9)	281(1)	302.4(8)	312.9(9)	335.3(8)	353(1)	365.3(8)
C_{22} (GPa)	247(1)	267(1)	279(1)	292(1)	308(1)	317(1)	328(1)
C_{33} (GPa)	274(1)	284.5(7)	300.6(6)	317.1(6)	332.2(6)	346.7(7)	360.1(6)
C_{44} (GPa)	85.8(7)	89.5(5)	94.3(5)	95.0(5)	97.4(5)	102.6(7)	107.1(5)
C_{55} (GPa)	69.3(5)	70.1(4)	73.5(3)	78.4(3)	76.6(3)	79.4(4)	82.4(3)
C_{66} (GPa)	93.0(7)	98.0(9)	100.5(7)	108.8(6)	109.4(7)	112(1)	115.2(9)
C_{12} (GPa)	85(1)	93(2)	108(1)	117(1)	130(1)	153(2)	165(1)
C_{13} (GPa)	66(1)	70.5(9)	79.8(8)	93.8(8)	99.2(7)	107.2(9)	116.8(7)
C_{23} (GPa)	87(2)	91(1)	96.5(9)	102(1)	113(1)	126(1)	134.6(9)
C_{15} (GPa)	5.4(7)	7.0(5)	6.9(4)	8.0(4)	10.3(4)	10.1(5)	8.9(4)
C_{25} (GPa)	17(1)	18(1)	27.3(8)	24.2(9)	22.2(7)	13(1)	10.3(9)
C_{35} (GPa)	28.7(6)	26.3(5)	27.4(4)	25.9(4)	26.8(4)	26.4(5)	26.7(3)
C_{46} (GPa)	14.6(6)	9.5(5)	12.0(4)	9.8(4)	11.6(5)	16.4(7)	17.5(5)
K_S^R (GPa)	135.9(7)	144.6(6)	155.2(4)	166.5(4)	179.1(4)	195.0(6)	206.4(4)
G^R (GPa)	82.7(3)	86.8(3)	89.5(3)	92.6(2)	95.2(3)	96.7(4)	99.1(3)
K_S^V (GPa)	140.1(7)	148.9(6)	161.2(4)	171.8(4)	184.5(4)	198.8(6)	209.7(4)
G^V (GPa)	86.3(3)	90.0(3)	93.5(3)	96.3(2)	98.9(3)	100.8(4)	103.4(3)
$K_S{}^{VRH}$ (GPa)	138(3)	147(3)	158(2)	169(3)	182(3)	197(2)	208(2)
G^{VRH} (GPa)	84(2)	88(2)	91(2)	94(2)	97(2)	99(2)	101(2)
Vp (km/s)	8.71(4)	8.86(3)	9.03(4)	9.18(3)	9.35(3)	9.53(3)	9.67(3)
Vs (km/s)	5.06(3)	5.12(3)	5.16(3)	5.19(3)	5.22(3)	5.23(3)	5.25(3)

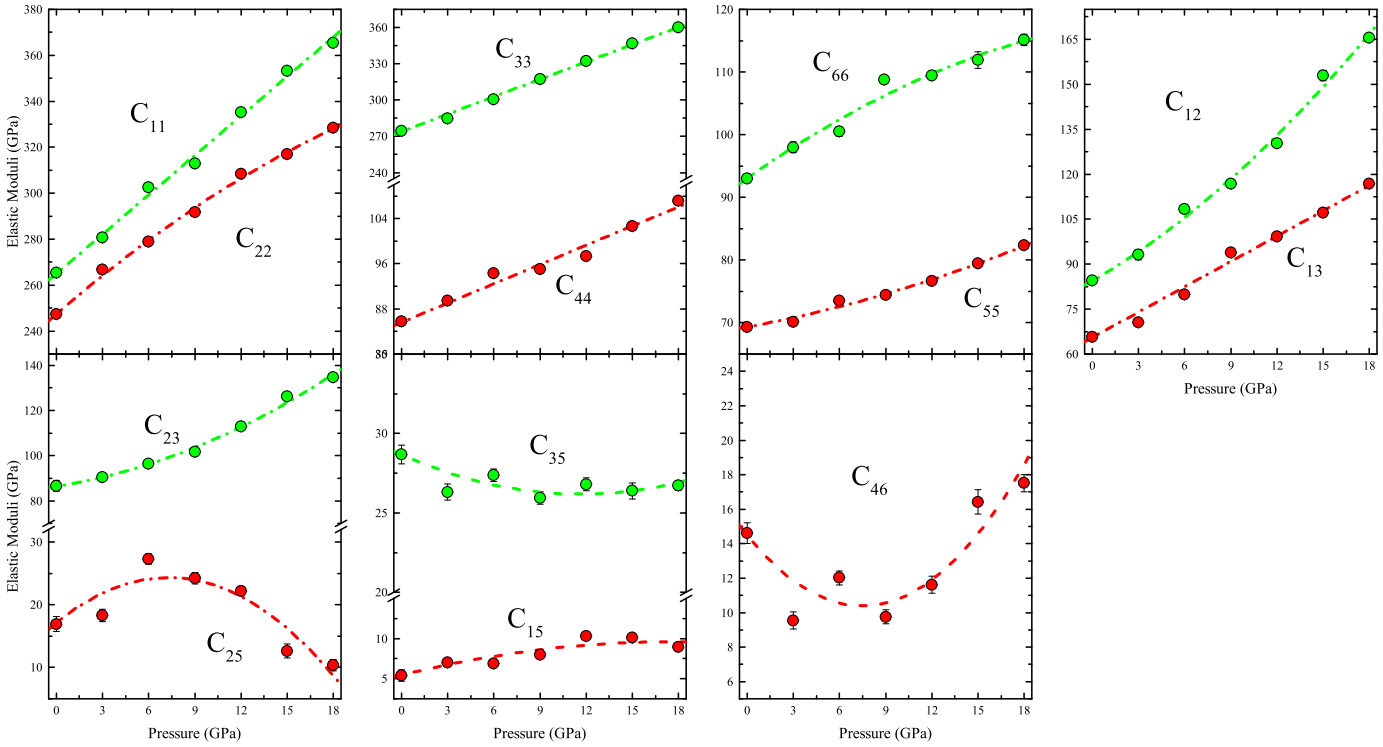

Fig. 3. Single-crystal elastic moduli of jadeite at high-P conditions. The dashed lines represent the best fit finite-strain elastic models.

the garnet (Figure S5). Overall, jadeite is among the fastest mineral phases in the Earth's upper mantle.

Fig. 3 shows the finite strain fitting results of all C_{ij}s. Those are the first experimentally determined values for jadeite under high-P conditions. Kawai and Tsuchiya (2010) and Walker (2012) obtained the C_{ij}s of jadeite at 0 K used first-principles calculations (Figure S6). Many of the computed C_{ij}s follow similar trends as the experimentally determined values in this study. For example, C_{11}, C_{22}, and C_{33} all increase with P; C_{33} is higher than C_{11} and C_{22} in the entire P range. However, it is also worth noting that the two computational studies at 0 K (Kawai and Tsuchiya, 2010; Walker, 2012) are not entirely consistent with each other. For some diagonal and off-diagonal C_{ij}s, such as C_{55}, C_{15}, C_{25}, and C_{35}, the two computational studies yield dramatically different results. It seems that the C_{25} and C_{35} values predicted by Kawai and Tsuchiya (2010) are closer to what were experimentally determined in this study, whereas the C_{55} calculated by Walker (2012) better matched the values measured in this study. Although both calculations were based on density functional theory, Kawai and Tsuchiya (2010) utilized the ab initio approach, whereas Walker (2012) utilized the

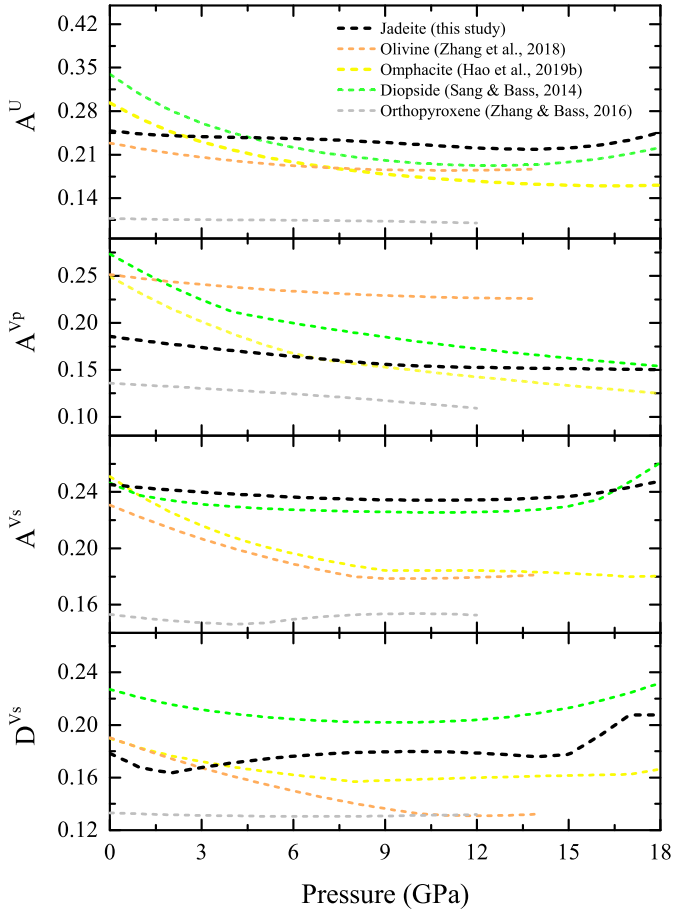

Fig. 4. The anisotropy indices (A^U, A^{Vp}, A^{Vs}, and D^{Vs}) of jadeite, diopside (Sang and Bass, 2014), omphacite (Hao et al., 2019b), orthopyroxene (Zhang and Bass, 2016), and olivine (Zhang et al., 2018).

plane wave and pseudopotentials in his calculation. These different technical treatments may contribute to the discrepancies shown in Figure S6. Further computational studies at higher Ts may help to resolve these issues.

3.3. Elastic anisotropy of jadeite at high-P conditions

Seismic anisotropy is a powerful tool for studying the flow field and identifying possible chemical heterogeneities in the Earth's upper mantle (Hao et al., 2019b). During the slab subduction, the flow-induced lattice preferred orientation of omphacite, which is the solid solution of jadeite and diopside, is the main contributor of the seismic anisotropy of slab crust (e.g. Zhang et al., 2006) due to the elastically isotropic nature of the garnet (e.g. Sinogeikin and Bass, 2000). As the primary phase up to 50 vol% in the subducted continental sediments/crust, determination of the elastic anisotropy of jadeite is also crucial for locating the enriched mantle reservoirs in the Earth's deep interior.

In this study, we used 4 different elastic anisotropy indices: Universal Anisotropy Index (A^U), the Vp and Vs azimuthal anisotropy A^{Vp} and A^{Vs}, and Vs polarization anisotropy D^{Vs} (Supporting Information, Text S1.4, Equation S6-S9) to describe the anisotropy of jadeite.

We calculated the anisotropy indices of jadeite up to 18 GPa and compared them with other major upper mantle anisotropic minerals (Fig. 4, Zhang et al., 2018; Sang and Bass, 2014; Zhang and Bass, 2016; Hao et al., 2019b). The P dependences of the C_{ij}s for all the other major upper mantle minerals can be found in Table S3. The decrease of the 4 anisotropy indices as a function of P is smaller for jadeite than the other minerals. When P exceeds ~5 GPa, the A^U of jadeite becomes the highest among all minerals. Olivine has the highest A^{Vp} in the entire P range. The A^{Vs} of jadeite remains the highest among all 5 minerals up to 16 GPa. Jadeite becomes more anisotropic in D^{Vs} than olivine and omphacite when P is higher than 4 GPa. These calculations suggest that the subducted sediments/crust can be highly anisotropic due to the enrichment of the jadeite component with strong intrinsic acoustic anisotropy.

3.4. Geophysical implications

Previous geochemical and petrological studies have suggested that the sediments/crust with continental origin may be recycled back into the deep mantle, down to perhaps the transition zone depth range (e.g. Chauvel et al., 1992; Liu et al., 2007). Due to the difference in major element composition, the seismic velocities of the subducted eclogitic oceanic crust, the subducted sediments/crust with continental origin, and the ambient mantle are different (Hao et al., 2019b; Irifune et al., 1994; Wu et al., 2009). In this study, utilizing the thermoelastic parameters of jadeite and other relevant mineral phases (Wu et al., 2009; Irifune et al., 1994), we modeled the density and velocities of the subducted sediments/crust with continental origin along 1000 K (cold) and 1600 K (ambient) mantle adiabats from 200 km to 500 km depth (Stixrude and Lithgow-Bertelloni, 2005; Katsura et al., 2010). In a realistic case, the geotherm may lie in between the two. We also compared our results with the velocities calculated for oceanic crust (Aoki and Takahashi, 2004), the global 1-D seismic model AK135 (Kennett et al., 1995), and the ambient pyrolitic mantle (Xu et al., 2008). Table S4 shows the thermoelastic parameters we used for all the relevant mineral phases. We adopted the experimentally constrained high-P petrological models by Aoki and Takahashi (2004) for the density and velocity calculation of the basaltic oceanic crust, Wu et al. (2009) and Irifune et al. (1994) for the subducted continent-derived sediments/crust. The mineral proportions, as well as compositions, are both calculated as depth-dependent (Fig. 5, Table S5). We assumed ideal mixing between different mineral endmembers. Voigt-Reuss-Hill averaging scheme is used for estimating the densities and elastic moduli of the multi-component lithologies (Supporting Information, Text S1.5 equation S10-S12). It is worth noting that the starting materials used in the 2 existing studies Irifune et al. (1994) and Wu et al. (2009) are similar yet both slightly different from the averaged upper continental crust composition (Rudnick and Fountain, 1995). The obtained petrological models of the subducted sediments/crust with continental origin are also different between Irifune et al. (1994) and Wu et al. (2009). In particular, the jadeite content in Irifune et al. (1994) decreased dramatically with P, and at 17 GPa it was less than 10 vol%. However, the jadeite content in Wu et al. (2009) was always higher than 30 vol%. In order to explore the effect of the small compositional difference of the starting materials on the high-P phase diagram of the continental sediments/crust (Irifune et al., 1994; Rudnick and Fountain, 1995; Wu et al., 2009), we performed additional PerpleX calculations to obtain the possible phase diagrams at high P-T conditions (Connolly, 2009; Supporting Information, Text S1.6, Figure S7). As shown in Figure S7, the calculated and experimentally determined jadeite volume proportion (~30%-50%) in Wu et al. (2009) is closer to the calculated value (~30%-39%) for the average upper continental crust (Rudnick and Fountain, 1995). However, due to the limitations of PerpleX software package (e.g. treatment of K), the calculation is still preliminary. It is also worth noting that the experimental run time in Wu et al. (2009) is significantly longer than Irifune et al. (1994). However, evaluating which petrological model is more reliable is beyond the scope of this study. Further high P-T phase equilibrium studies are needed to clarify the discrepancies between the

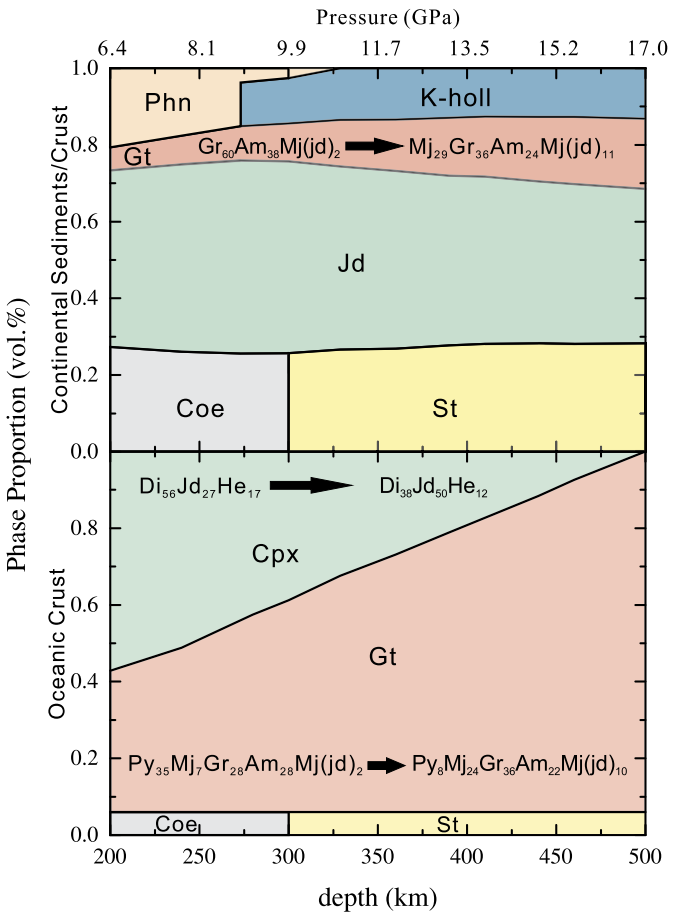

Fig. 5. Phase proportions of the continental sediments/crust (Wu et al., 2009) and the oceanic crust (Aoki and Takahashi, 2004) as a function of depth (Coe: coesite; St: stishovite; Gt: garnet; Py: pyrope; Mj: majorite; Gr: grossular; Am: almandine; Mj(jd): jadeite-majorite; Cpx: clinopyroxene; Di: diopside; Jd: jadeite; He: hedenbergite; Phn: phengite; K-holl: K-hollandite).

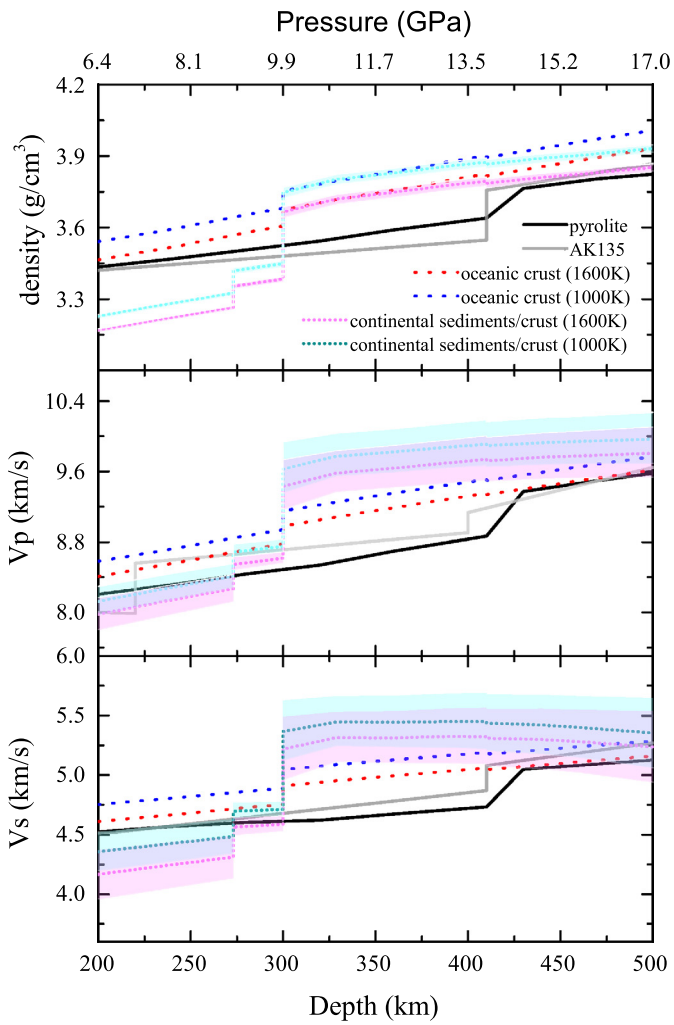

Fig. 6. The density and seismic velocities of the subducted continental sediments/crust and oceanic crust, compared with the pyrolite model (Xu et al., 2008), and AK 135 model (Kennett et al., 1995). The blue and pink regions are bounded by Voigt and Reuss bounds at 1000 K and 1600 K adiabat, respectively. (For interpretation of the colors in the figure(s), the reader is referred to the web version of this article.)

2 existing studies. In this study, we calculated the high P-T seismic properties of the continental sediments/crust based on both Wu et al. (2009) and Irifune et al. (1994), shown as Fig. 6 and Figure S8 in the Supporting Information, respectively. The differences in terms of seismic properties are small between the two models, and we focus on discussing the results based on the Wu et al. (2009) in the remainder of the text.

As shown in Fig. 6, at depths shallower than ~300 km, the density of the continent-derived sediments/crust is significantly less than the oceanic crust and the ambient mantle. This is caused by the low densities of jadeite, phengite, and coesite compared with the major upper mantle mineral phases, such as olivine and garnet (Zhang et al., 2018; Chen et al., 2017). Although the seismic velocities of phengite and coesite in the continental sediments/crust are much slower than the most abundant upper mantle mineral olivine (Zhang et al., 2018; Chen et al., 2017; Vaughan and Guggenheim, 1986), the high jadeite content in the continental sediments/crust results in the similar Vp of the continental sediments/crust and the ambient mantle. On the other hand, the Vs of the continental sediments/crust is significantly lower than the ambient mantle. Thus, the elevated Vp/Vs values (1.88-1.92) are expected in regions enriched in continentally derived sediments/crust. This can be used as an alternative explanation for the high Vp/Vs regions in the shallower upper mantle in addition to partial melt (e.g. Nakajima et al., 2001).

At the depth ~300 km, the phase transformation from coesite to stishovite causes the density and velocity jumps observed for both the continent-derived sediments/crust and oceanic crust (Chen et al., 2017; Yang and Wu, 2014). Due to the high silica content (>25 vol%), the density of the continental sediments/crust is similar to oceanic crust and higher than the ambient mantle. However, the density of oceanic crust exceeds that of the continent-derived sediments/crust at ~350 km depth because of the dissolution of Cpx into garnet (Aoki and Takahashi, 2004), though both of them are denser than the ambient mantle. The seismic velocities of the continent-derived sediments/crust increase by 9.5% and 13.8% for Vp and Vs, respectively at ~300 km depth. This velocity jump and the high volume fraction of jadeite make the continental sediments/crust the fastest petrological component in the deep upper mantle. Assuming the continent-derived sediments/crust are at the same T as the ambient mantle (along the 1600 K adiabat geotherm), the Vp and Vs difference between the continental sediments/crust and the ambient mantle can be as high as 11.8% and 14.7%, respectively at 300-410 km depth. If we consider the possibly lower T of the continental sediments/crust, then the maximum velocity contrast will be bracketed between 11.8%-13.9% and 14.7%-17.5% for Vp and Vs, respectively. The Vp and Vs of continent-derived sediments/crust are also 5.6% and 7.3% faster than those of the subducted oceanic crust.

At ~410 km depth, the density, Vp, and Vs of the ambient mantle increase by 2.9%, 5.0%, and 6.2%, respectively, due to the olivine to wadsleyite phase transformation (Xu et al., 2008). As a result, the density contrast between the ambient mantle, continental sediments/crust, and oceanic crust decreases to as small as 1.4%. The seismic velocities of the ambient mantle are similar to oceanic crust. The Vp and Vs of the continental sediments/crust are still significantly faster than the ambient mantle by 4.1% and 5.0%, respectively. At this depth, the Vs of the continental sediments/crust decrease with depth, because of the computationally predicted softening of the elastic properties of K-hollandite at 0 K (Kawai and Tsuchiya, 2013). Future experimental investigations may help us further understand this interesting beheavior.

As discussed above, the subducted continental sediments/crust are extremely fast between 300 km to 500 km depth. The fast seismic anomalies observed in the upper mantle can be easily explained by the existence of the recycled continental sediments/crust even without the need of any abnormal cold Ts. For example, the fast seismic anomalies at 300-550 km depth under Central Asia (Kufner et al., 2016) are as high as 4% for Vp, which requires >1000 K T difference assuming a pure thermal origin. However, a T of more than 1000 K lower than the surrounding mantle seems unrealistic. Considering the possible subduction of continental crust under the Tibetan plateau (e.g. Replumaz et al., 2010), this 4% Vp anomaly can easily be explained by ~34% continental crust at the same T with the ambient mantle or ~29% continental crust at about 200-300 K lower T. In addition, a few distinct enriched geochemical reservoirs have been identified under the South Pacific Ocean from previous studies (Hofmann, 1997), which is in agreement with the fast anomalies identified in global P-wave tomography models in the deep upper mantle (e.g. Li et al., 2008).

4. Conclusions

We have determined the thermal EOS and the single-crystal elastic properties of jadeite by synchrotron single-crystal XRD and Brillouin spectroscopy. The derived thermoelastic properties for jadeite are: K_{T0}=134.6 GPa, K'_{T0}=3.8(2), α_0=3.4(5) $\times 10^{-5}$ K^{-1}, K_{S0}=138(3) GPa, G_0=84(2) GPa, K'_{S0}=3.9(1), and G'_0=1.09(4). In the entire stability P range, the acoustic velocities of jadeite are faster than all the other Cpx. Based on the modeled density and seismic velocities of the subducted sediments/crust with continental origin, we found that the seismic velocities of the continental sediments/crust are faster than the ambient upper mantle by ~11.8% and ~14.7% at depths greater than ~300 km for Vp and Vs, respectively. This huge velocity contrast can help to identify the enriched geochemical reservoirs and heterogeneities in the Earth's interior.

Declaration of competing interest

The authors declare that they have no known competing financial interests or personal relationships that could have appeared to influence the work reported in this paper.

Acknowledgements

The authors would like to thank Mike Spilde for the help with Electron Microprobe Analysis experiments at the Institute of Meteoritics at UNM and Sergey Tkachev for the Neon gas loading of the DACs at GSECARS, APS, ANL. The use of the gas-loading system and 13-BM-C beamlines are supported by COMPRES, the Consortium for Materials Properties Research in Earth Sciences under NSF Cooperative Agreement EAR 1661511, and GSECARS is funded by NSF (EAR - 1634415) and Department of Energy (DOE) – GeoSciences (DE-FG02-94ER14466). This research used resources of the APS, a U.S. DOE Office of Science User Facility operated for the DOE Office of Science by ANL under Contract NO. DE-AC02-06CH11357. The X-ray Atlas instrument at the University of Hawaii was funded by NSF grant EAR 1541516 (PD). All the data presented in this study are available in the Supporting Information. We thank Suyu Fu for providing the original Matlab code for the C_{ij} sensitivity test and Brandon Schmandt for the insightful discussions with geophysical implications.

Funding: This work is supported by the National Science Foundation (NSF) under Grant EAR 1646527 (JZ) and the start-up fund from UNM (JZ). PD was supported by NSF grant EAR 1722969.

Appendix A. Supplementary material

Supplementary material related to this article can be found online at https://doi.org/10.1016/j.epsl.2020.116345.

References

Angel, R.J., Alvaro, M., Nestola, F., 2018. 40 years of mineral elasticity: a critical review and a new parameterisation of equations of state for mantle olivines and diamond inclusions. Phys. Chem. Miner. 45 (2), 95–113. https://doi.org/10.1007/s00269-017-0900-7.

Aoki, I., Takahashi, E., 2004. Density of MORB eclogite in the upper mantle. Phys. Earth Planet. Inter. 143, 129–143. https://doi.org/10.1016/j.pepi.2003.10.007.

Arevalo Jr, R., McDonough, W.F., Luong, M., 2009. The K/U ratio of the silicate Earth: insights into mantle composition, structure and thermal evolution. Earth Planet. Sci. Lett. 278 (3–4), 361–369. https://doi.org/10.1016/j.epsl.2008.12.023.

Cameron, M., Sueno, S., Prewitt, C.T., Papike, J.J., 1973. High-temperature crystal chemistry of acmite, diopside, hedenbergite jadeite, spodumene and ureyite. Am. Mineral.: J. Earth Planet. Mater. 58 (7–8), 594–618.

Chauvel, C., Hofmann, A.W., Vidal, P., 1992. HIMU-EM: the French Polynesian connection. Earth Planet. Sci. Lett. 110 (1–4), 99–119. https://doi.org/10.1016/0012-821X(92)90042-T.

Chen, T., Liebermann, R.C., Zou, Y., Li, Y., Qi, X., Li, B., 2017. Tracking silica in Earth's upper mantle using new sound velocity data for coesite to 5.8 GPa and 1073 K. Geophys. Res. Lett. 44 (15), 7757–7765. https://doi.org/10.1002/2017GL073950.

Connolly, J.A.D., 2009. The geodynamic equation of state: what and how. Geochem. Geophys. Geosyst. 10 (10). https://doi.org/10.1029/2009GC002540.

Corgne, A., Keshav, S., Fei, Y., McDonough, W.F., 2007. How much potassium is in the Earth's core? New insights from partitioning experiments. Earth Planet. Sci. Lett. 256 (3–4), 567–576. https://doi.org/10.1016/j.epsl.2007.02.012.

Davies, G.F., Dziewonski, A.M., 1975. Homogeneity and constitution of the Earth's lower mantle and outer core. Phys. Earth Planet. Inter. 10 (4), 336–343. https://doi.org/10.1016/0031-9201(75)90060-6.

Dera, P., Zhuravlev, K., Prakapenka, V., Rivers, M.L., Finkelstein, G.J., Grubor-Urosevic, O., et al., 2013. High pressure single-crystal micro X-ray diffraction analysis with GSE_ADA/RSV software. High Press. Res. 33 (3), 466–484. https://doi.org/10.1080/08957959.2013.806504.

Fei, Y., Ricolleau, A., Frank, M., Mibe, K., Shen, G., Prakapenka, V., 2007. Toward an internally consistent pressure scale. Proc. Natl. Acad. Sci. 104 (22), 9182–9186. https://doi.org/10.1073/pnas.0609013104.

Hao, M., Pierotti, C.E., Tkachev, S., Prakapenka, V., Zhang, J.S., 2019a. The single-crystal elastic properties of the jadeite-diopside solid solution and their implications for the composition-dependent seismic properties of eclogite. Am. Mineral. 104 (7), 1016–1021. https://doi.org/10.2138/am-2019-6990.

Hao, M., Zhang, J.S., Pierotti, C.E., Ren, Z., Zhang, D., 2019b. High-pressure single-crystal elasticity and thermal equation of state of omphacite and their implications for the seismic properties of eclogite in the Earth's interior. J. Geophys. Res., Solid Earth 124 (3), 2368–2377. https://doi.org/10.1029/2018JB016964.

Hofmann, A.W., 1997. Mantle geochemistry: the message from oceanic volcanism. Nature 385 (6613), 219. https://doi.org/10.1038/385219a0.

Holland, T.J.B., Powell, R., 2011. An improved and extended internally consistent thermodynamic dataset for phases of petrological interest, involving a new equation of state for solids. J. Metamorph. Geol. 29 (3), 333–383. https://doi.org/10.1111/j.1525-1314.2010.00923.x.

Irifune, T., Ringwood, A.E., Hibberson, W.O., 1994. Subduction of continental crust and terrigenous and pelagic sediments: an experimental study. Earth Planet. Sci. Lett. 126 (4), 351–368. https://doi.org/10.1016/0012-821X(94)90117-1.

Kandelin, J., Weidner, D.J., 1988. The single-crystal elastic properties of jadeite. Phys. Earth Planet. Inter. 50 (3), 251–260. https://doi.org/10.1016/0031-9201(88)90106-9.

Katsura, T., Yoneda, A., Yamazaki, D., Yoshino, T., Ito, E., 2010. Adiabatic temperature profile in the mantle. Phys. Earth Planet. Inter. 183 (1–2), 212–218. https://doi.org/10.1016/j.pepi.2010.07.001.

Kawai, K., Tsuchiya, T., 2010. Ab initio investigation of high-pressure phase relation and elasticity in the $NaAlSi_2O_6$ system. Geophys. Res. Lett. 37 (17). https://doi.org/10.1029/2010GL044310.

Kawai, K., Tsuchiya, T., 2013. First-principles study on the high-pressure phase transition and elasticity of $KAlSi_3O_8$ hollandite. Am. Mineral. 98 (1), 207–218. https://doi.org/10.2138/am.2013.4077.

Kawai, K., Tsuchiya, T., 2015. Elasticity of continental crust around the mantle transition zone. In: The Earth's Heterogeneous Mantle. Springer, Cham, pp. 259–274.

Kennett, B.L., Engdahl, E.R., Buland, R., 1995. Constraints on seismic velocities in the Earth from traveltimes. Geophys. J. Int. 122 (1), 108–124. https://doi.org/10.1111/j.1365-246X.1995.tb03540.x.

Kufner, S.K., Schurr, B., Sippl, C., Yuan, X., Ratschbacher, L., Ischuk, A., Tilmann, F., 2016. Deep India meets deep Asia: lithospheric indentation, delamination and break-off under Pamir and Hindu Kush (Central Asia). Earth Planet. Sci. Lett. 435, 171–184. https://doi.org/10.1016/j.epsl.2015.11.046.

Li, B., Neuville, D.R., 2010. Elasticity of diopside to 8 GPa and 1073 K and implications for the upper mantle. Phys. Earth Planet. Inter. 183 (3–4), 398–403. https://doi.org/10.1016/j.pepi.2010.08.009.

Li, C., van der Hilst, R.D., Engdahl, E.R., Burdick, S., 2008. A new global model for P wave speed variations in Earth's mantle. Geochem. Geophys. Geosyst. 9 (5).

Liu, L., Zhang, J., Green II, H.W., Jin, Z., Bozhilov, K.N., 2007. Evidence of former stishovite in metamorphosed sediments, implying subduction to >350 km. Earth Planet. Sci. Lett. 263 (3–4), 180–191. https://doi.org/10.1016/j.epsl.2007.08.010.

Mao, H.K., Bell, P.M., Shaner, J.T., Steinberg, D.J., 1978. Specific volume measurements of Cu, Mo, Pd, and Ag and calibration of the ruby R_1 fluorescence pressure gauge from 0.06 to 1 Mbar. J. Appl. Phys. 49 (6), 3276–3283. https://doi.org/10.1063/1.325277.

McCarthy, A.C., Downs, R.T., Thompson, R.M., 2008. Compressibility trends of the clinopyroxenes, and in-situ high-pressure single-crystal X-ray diffraction study of jadeite. Am. Mineral. 93 (1), 198–209. https://doi.org/10.2138/am.2008.2521.

Nakajima, J., Matsuzawa, T., Hasegawa, A., Zhao, D., 2001. Three-dimensional structure of Vp, Vs, and Vp/Vs beneath northeastern Japan: implications for arc magmatism and fluids. J. Geophys. Res., Solid Earth 106 (B10), 21843–21857. https://doi.org/10.1029/2000JB000008.

Nestola, F., Ballaran, T.B., Liebske, C., Bruno, M., Tribaudino, M., 2006. High-pressure behaviour along the jadeite $NaAlSi_2O_6$–aegirine $NaFeSi_2O_6$ solid solution up to 10 GPa. Phys. Chem. Miner. 33 (6), 417–425. https://doi.org/10.1007/s00269-006-0089-7.

Norris, S., 2008. Elastic properties of jadeite. Undergraduate Senior thesis. University of Illinois.

Pandolfo, F., Cámara, F., Domeneghetti, M.C., Alvaro, M., Nestola, F., Karato, S.I., Amulele, G., 2015. Volume thermal expansion along the jadeite–diopside join. Phys. Chem. Miner. 42 (1), 1–14. https://doi.org/10.1007/s00269-014-0694-9.

Posner, E.S., Dera, P., Downs, R.T., Lazarz, J.D., Irmen, P., 2014. High-pressure single-crystal X-ray diffraction study of jadeite and kosmochlor. Phys. Chem. Miner. 41 (9), 695–707. https://doi.org/10.1007/s00269-014-0684-y.

Replumaz, A., Negredo, A.M., Villasenor, A., Guillot, S., 2010. Indian continental subduction and slab break-off during Tertiary collision. Terra Nova 22 (4), 290–296. https://doi.org/10.1111/j.1365-3121.2010.00945.x.

Rudnick, R.L., Fountain, D.M., 1995. Nature and composition of the continental crust: a lower crustal perspective. Rev. Geophys. 33 (3), 267–309. https://doi.org/10.1029/95RG01302.

Sang, L., Bass, J.D., 2014. Single-crystal elasticity of diopside to 14 GPa by Brillouin scattering. Phys. Earth Planet. Inter. 228, 75–79. https://doi.org/10.1016/j.pepi.2013.12.011.

Sinogeikin, S.V., Bass, J.D., 2000. Single-crystal elasticity of pyrope and MgO to 20 GPa by Brillouin scattering in the diamond cell. Phys. Earth Planet. Inter. 120 (1–2), 43–62. https://doi.org/10.1016/S0031-9201(00)00143-6.

Stixrude, L., Lithgow-Bertelloni, C., 2005. Thermodynamics of mantle minerals—I. Physical properties. Geophys. J. Int. 162 (2), 610–632. https://doi.org/10.1111/j.1365-246X.2005.02642.x.

Tribaudino, M., Nestola, F., Bruno, M., Ballaran, T.B., Liebske, C., 2008. Thermal expansion along the $NaAlSi_2O_6$–$NaFe^{3+}Si_2O_6$ and $NaAlSi_2O_6$–$CaFe^{2+}Si_2O_6$ solid solutions. Phys. Chem. Miner. 35 (5), 241–248. https://doi.org/10.1007/s00269-008-0217-7.

Vaughan, M.T., Guggenheim, S., 1986. Elasticity of muscovite and its relationship to crystal structure. J. Geophys. Res., Solid Earth 91 (B5), 4657–4664. https://doi.org/10.1029/JB091iB05p04657.

Walker, A.M., 2012. The effect of pressure on the elastic properties and seismic anisotropy of diopside and jadeite from atomic scale simulation. Phys. Earth Planet. Inter. 192, 81–89. https://doi.org/10.1016/j.pepi.2011.10.002.

Wu, Y., Fei, Y., Jin, Z., Liu, X., 2009. The fate of subducted upper continental crust: an experimental study. Earth Planet. Sci. Lett. 282 (1–4), 275–284. https://doi.org/10.1016/j.epsl.2009.03.028.

Xu, W., Lithgow-Bertelloni, C., Stixrude, L., Ritsema, J., 2008. The effect of bulk composition and temperature on mantle seismic structure. Earth Planet. Sci. Lett. 275 (1–2), 70–79. https://doi.org/10.1016/j.epsl.2008.08.012.

Yang, R., Wu, Z., 2014. Elastic properties of stishovite and the $CaCl_2$-type silica at the mantle temperature and pressure: an ab initio investigation. Earth Planet. Sci. Lett. 404, 14–21. https://doi.org/10.1016/j.epsl.2014.07.020.

Zhang, J.S., Bass, J.D., 2016. Single-crystal elasticity of natural Fe-bearing orthoenstatite across a high-pressure phase transition. Geophys. Res. Lett. 43 (16), 8473–8481. https://doi.org/10.1002/2016GL069963.

Zhang, J.S., Bass, J.D., Schmandt, B., 2018. The elastic anisotropy change near the 410-km discontinuity: predictions from single-crystal elasticity measurements of olivine and wadsleyite. J. Geophys. Res., Solid Earth 123 (4), 2674–2684. https://doi.org/10.1002/2017JB015339.

Zhang, J., Green II, H.W., Bozhilov, K.N., 2006. Rheology of omphacite at high temperature and pressure and significance of its lattice preferred orientations. Earth Planet. Sci. Lett. 246 (3–4), 432–443. https://doi.org/10.1016/j.epsl.2006.04.006.

Zhao, Y., Von Dreele, R.B., Shankland, T.J., Weidner, D.J., Zhang, J., Wang, Y., Gasparik, T., 1997. Thermoelastic equation of state of jadeite $NaAlSi_2O_6$: an energy-dispersive reitveld refinement study of low symmetry and multiple phases diffraction. Geophys. Res. Lett. 24 (1), 5–8. https://doi.org/10.1029/96GL03769.